PCCP

PAPER

View Article Online
View Journal | View Issue

Cite this: *Phys. Chem. Chem. Phys.*, 2017, **19**, 2409

Excited state proton transfer in 2′-hydroxychalcone derivatives†

Michael Dommett and Rachel Crespo-Otero*

Received 3rd November 2016,
Accepted 22nd December 2016

DOI: 10.1039/c6cp07541j

www.rsc.org/pccp

Fluorophores exhibiting excited-state intramolecular proton transfer (ESIPT) are promising candidates for applications ranging from imaging and probing to laser dyes, optoelectronic devices and molecular logic gates. Recently, ESIPT-active solid-state emitters based on 2′-hydroxychalcone have been synthesized. The compounds are almost non-emissive in solution but emit in the deep red/NIR region when crystalline. Herein, we present a comprehensive theoretical investigation of the gas-phase excited state relaxation pathways in five 2′-hydroxychalcone systems, using a combination of static and non-adiabatic simulations. We identify two competing non-radiative relaxation channels, driven by intramolecular rotation in the enol and keto excited states. Both mechanisms are accessible for the five compounds studied and their relative population depends on the nature of the substituent. The addition of electron-donating substituents greatly increases the propensity of the ESIPT pathway *versus* rotation in the enol state. The identification of the fundamental relaxation mechanisms is the first step towards understanding the aggregated emission phonomena of these compounds.

Introduction

Organic compounds which emit in the near infra-red region (NIR) have garnered much attention in recent years due to their potential applications in bioimaging, molecular probes, and organic light-emitting diodes (OLEDs).[1–3] A promising class of NIR emitting candidates are those exhibiting excited state intramolecular proton transfer (ESIPT). ESIPT involves tautomerism between enol and keto states in a fully reversible four-level photocycle, mediated by an intramolecular hydrogen bond. Emission can occur from either or both of the excited enol (E*) or keto (K*) states, dependent on external factors such as solvent polarity and viscosity.[4–7] Emission from K* results in a remarkable Stokes shift, preventing self-absorption and increasing the quantum yield of these systems.

For most ESIPT processes containing strong hydrogen bonds, proton transfer is near barrierless and occurs on a femtosecond time scale.[8] The rate of the proton transfer and nature of fluorescence are highly sensitive to the surrounding medium and the presence of electron donor/acceptor moieties, making ESIPT species attractive fluorophores for applications ranging from imaging and probing to laser dyes, optoelectronic devices and molecular logic gates.[4,9–12]

Hindering progress in the realization of NIR devices is the phenomenon of aggregation-caused quenching, where fluorescence in the solid state is reduced compared to solution. NIR compounds typically contain extended π-conjugated frameworks, where face to face stacking of aromatic groups mediates fluorescence quenching through excimer and exciplex formation.[13] To overcome this, researchers have adopted aggregation induced emission (AIE) and aggregation induced enhanced emission strategies to design molecules which are brightly fluorescent in the solid state. Such strategies involve the restriction of non-radiative relaxation pathways, such as intramolecular rotation and *cis–trans* isomerisation.[13–20]

2′-Hydroxychalcones (Fig. 1) are ESIPT-active compounds demonstrating NIR emission and have been utilized as molecular probes in enzyme and latent fingerprint detection.[21–27]

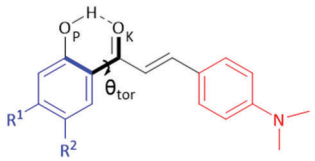

Fig. 1 The structures of 2′-hydroxychalcone compounds **1–5** investigated in this work. Important atoms are numbered, θ_{tor} is the torsional rotation mode discussed herein (**1**: R^1 = H, R^2 = H; **2**: R^1 = CH_3, R^2 = H, **3**: R^1 = OCH_3, R^2 = H, **4**: R^1 = H, R^2 = CH_3, **5**: R^1 = H, R^2 = OCH_3). To aid discussion, the blue ring (left) denotes fragment **A**, whilst red (right) represents fragment **B**.

Recently, 2′-hydroxychalcone derivatives displaying AIE have been synthesized, with potential for lasing applications.[28] The compounds are almost non-emissive in solution but emit in the deep red/NIR region when crystalline. The AIE characteristics

School of Biological and Chemical Sciences, Materials Research Institute, Queen Mary University of London, Mile End Road, London E1 4NS, UK.
E-mail: r.crespo-otero@qmul.ac.uk

† Electronic supplementary information (ESI) available. See DOI: 10.1039/c6cp07541j

depend on a subtle balance of effects which are, as yet, not well understood. The presence of an intramolecular H-bond and a donor–acceptor skeleton, the position of the phenol ring substituents, the conformation of the molecule and the molecular packing modes all confer the quantum yield of the system. In particular, high planarity and edge-to-face packing are essentials for emission in the solid state.[28]

Experimentally, compounds **1–5** are non-emissive in solution (Fig. 1). However, in crystalline form, compounds **1–3** emit brightly in the NIR region. Compounds **4** and **5**, with substitution at the *para* position relative to the hydroxyl group, are dark in solution and solid state. An open question is whether substituents modify the photo-deactivation mechanisms. Excited state calculations of the molecules allow isolation of the effect of the substituents and identification of the main deactivation mechanisms, which could be inaccessible in the solid state. This paper focuses on the analysis of the electronic effects on the individual fluorophores, a crucial first step towards understanding the effect of aggregation on the photochemistry of these molecules.

We present an in-depth theoretical study of the gas phase photochemistry of five 2′hydroxychalcone derivatives, based upon substitution of electron donating groups at the *meta* and *para* positions of the phenol ring. We analyse the effect of the substituents on the four level photocycle and employ non-adiabatic dynamics to investigate the relaxation mechanisms and the competition between different deactivation channels. These simulations show that a strong electron donating group (EDG) such as methoxy alters the topology of the potential energy surface (PES), destabilising the E* state; assisting and accelerating proton transfer. Our results provide detailed understanding into the fundamental relaxation mechanisms of 2′-hydroxychalcones and the role of the substituents, which is the initial step to unravel the effect of aggregation on the emission properties.

Computational details

The ground state geometries of all the compounds were optimised in vacuum using resolution of identity MØller Plesset to the second order (MP2)[29] with the def2-SV(P) and def2-TZVP basis sets.[30,31] Vertical excitation energies were calculated in vacuum using coupled cluster to approximated second order (CC2) and algebraic diagrammatic construction to the second order (ADC(2)) methods under the resolution of identity approximation.[32–36] Core electrons were frozen for all MP2, ADC(2) and CC2 calculations. We compare the performance of the ADC(2) and CC2 methods and consider the effect basis set in the case of ADC(2). ADC(2) and CC2 methods offer a computationally efficient route to recovering electron correlation, with equilibrium properties comparing favourably with CCSD.[36]

Geometry optimization in the first excited state was carried out in vacuum for **1–5** with ADC(2) and CC2 methods using the same basis sets as the ground state optimization. These calculations were performed with Turbomole v7.0.[37] The level of theory considered to discuss the features of the PESs is CC2/def2-TZVP, unless otherwise is specified in the text.

The CIOpt software package of Levine, Coe and Martinez was used to determine the location of the minimal energy conical intersection (MECI) structures based on the Lagrange multiplier technique.[38] The algorithm does not require the non-adiabatic couplings. We employ a version of the program adapted for use with Turbomole.[39] The MECI structures were obtained for **1–5** at the CC2/def2-TZVP, ADC(2)/def2-TZVP and ADC(2)/def2-SV(P) levels of theory with α = 0.02 Hartree. In the case of **1**, complete active state self-consistent (CASSCF) calculations were performed with MOLPRO program.[40] The S_0/S_1 conical intersections were optimised with state-average (SA) complete active space self-consistent field (CASSCF). The active space considered 12 electrons in 11 orbitals including 2 states in the average with the 6-31G(d) basis set. For the K S_1/S_0 MECI, the CASSCF(14,13) active space was also considered. The active space includes the π orbitals with larger occupations and the $nO_P + nO_K$ orbital (all orbitals are shown in the ESI†).

The PESs were explored through linear interpolation (LIIC) pathways with ADC(2)/def2-TZVP level of theory. In the case of **1**, the intermediate LIIC geometries were relaxed considering the θ_{tor} angle fixed at the CC2/def2-TZVP level of theory. The geometries along the seam were located using CIOpt.

The absorption spectra of **1–5** were simulated using the nuclear ensemble method. 500 nuclear configurations were generated based on a Wigner distribution of the harmonic frequencies calculated at MP2/def2-SV(P) level of theory.[41] Five excited states at ADC(2)/def2-SV(P) level of theory were calculated for each individual geometry. For **1** and **5**, surface hopping non-adiabatic dynamics simulations were performed using NEWTON-X[42,43] interfaced with Turbomole, at ADC(2)/def2-SV(P) level of theory. The exploration of the potential energy surfaces showed that ESIPT is barrierless, thus tunnelling is not expected to be important for the photo-relaxation of these compounds. The surface hopping method is able to describe proton transfer in a ballistic regime.

The initial conditions were generated from the absorption spectra considering an energy window of 0.15 eV, which simulates the effect of excitation with a laser.[44] The geometries contributing to these energy windows were used as initial conditions for the trajectory propagation along with their momenta.[41,42,44,45] Three excited states were considered; the ground state, S_1, and the closely lying S_2.

For compound **1**, an energy window at absorption maximum of 3.29 $\pm$ 0.15 eV was selected. 50 trajectories were statistically distributed between S_1 (30) and S_2 (20), according to their oscillator strengths. The same protocol was used for compound **5**, with 50 trajectories (S_1: 30 and S_2: 20) from an energy window of 3.35 $\pm$ 0.15 eV. The maximum simulation time was 500 fs, with a time step of 0.5 fs and the quantum equations were integrated with 0.025 fs using interpolated quantities between classical steps. Non-adiabatic effects were included using the fewest-switches surface hopping algorithm with decoherence corrections (α = 0.1 Hartree).[42] Non-adiabatic couplings between S_2 and S_1 were estimated approximately using an approximated wave-function and the numerical method proposed by Izmaylov *et al.*[46–48] The trajectories were terminated when the energy gap

between S_1 and S_0 was smaller than 0.1 eV. This strategy provides an estimation of the S_1/S_0 crossing times.[49]

Results and discussion

The analysis of the potential energy surfaces of 2′-hydroxychalcones derivatives helps understand their photochemistry. Herein, we analyse the effect of substituents on the four energy level cycle. We found two competing relaxation pathways associated with the E* and K* states. The presence of two accessible S_0/S_1 MECI for all compounds (**1–5**) explains the quenching of fluorescence in the gas phase.

In the next sections, we analyse in-depth the effect of the substituents on the stability of the E* and K* minima and MECI structures. We also consider the performance of ADC(2) and CC2 levels of theory in the description of the photochemistry of these molecules.

Fig. 2 illustrates the effect of the substituents on the energy levels for the five compounds studied (**1–5**). An EDG group in *para* destabilises the E* state, producing a bias toward the ESIPT mechanism. Further exploration of the potential energy surfaces of **1** and **5** using non-adiabatic dynamics simulations confirms this hypothesis.

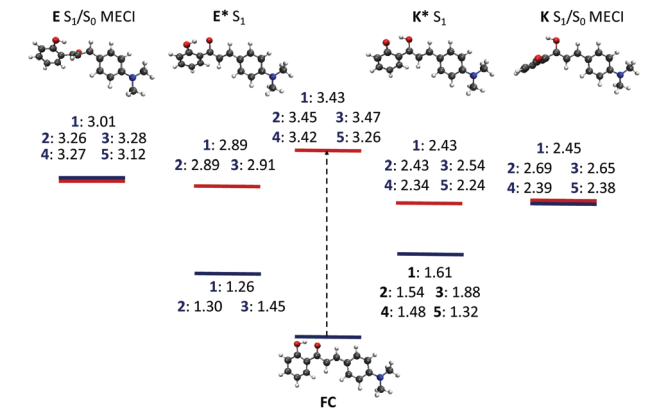

Fig. 2 Relative energies (in eV) for all derivatives calculated at CC2/def2-TZVP level of theory. In all cases, the energy of the ground state was taken as reference.

Vertical excitations

The vertical excitation energies for the first three excited states were calculated for structures **1–5**. Table 1 summarises the results of excitation to S_1 and S_2 (details for all vertical excitations can be found in the ESI†). The first excited state is bright, showing a minimal influence of the substituent for **1–4**, which vary by less than 0.05 eV across the four structures and two methods. In the case of **5**, there is a slight shift to the red.

Comparing the performance of ADC(2) and CC2 methods, when the same basis set is used (def2-TZVP), ADC(2) vertical excitations energies are about 0.1 eV deviated to the red with respect to the CC2 values. In the case of ADC(2), the def2-SV(P) basis set shifts the energies to the blue by about 0.1 eV. The simulation of the spectra at the ADC(2)/def2-SV(P) level of theory showed a red shift of 0.1–0.2 eV due to vibrational broadening. Similar shifts are expected for all levels of theory.

Table 1 Vertical excitations for the first two excited states for compounds **1–5** obtained at ADC(2)/def2-TZVP and CC2/def2-TZVP levels of theory

	ADC(2)/def2-SV(P)		ADC(2)/def2-TZVP		CC2/def2-TZVP	
	S_1	S_2	S_1	S_2	S_1	S_2
1	3.53	3.58	3.36	3.44	3.43	3.67
2	3.53	3.59	3.38	3.46	3.45	3.68
3	3.59	3.64	3.40	3.51	3.47	3.75
4	3.53	3.57	3.36	3.42	3.42	3.65
5	3.42	3.52	3.20	3.39	3.26	3.54

The calculated excitation energies at all considered levels of theory are in good agreement with the reported experimental values of 3.32, 2.82 and 3.03 eV in the crystal, and in the solvents DCM and hexane respectively.[3] In the case of **1**, the excitation energies obtained at ADC(2)/def2-TZVP level of theory considering DCM and hexane as a continuum are 3.29 and 3.15 eV respectively. These calculations show that a polar environment shifts S_1 to the red. The interaction with a second molecule has a similar effect on the vertical excitations shifting the energies to the red (ESI†).

The first excitation is predominantly HOMO–LUMO and of ππ* character. The effect of substituent on the electron density is only evident when a methoxy group in the *para* position (compound **5**). Excitation to the close lying dark S_2 state for **1–4** is predicted to be of nπ* character, with contributions from nO_P and nO_K (Section S2, ESI†). For **1–4**, in the ground state, significant electron density is located on the **B** fragment due to the amine group. Excitation to S_1 transfers electron density from **B** to the conjugated bridge (Fig. 3).

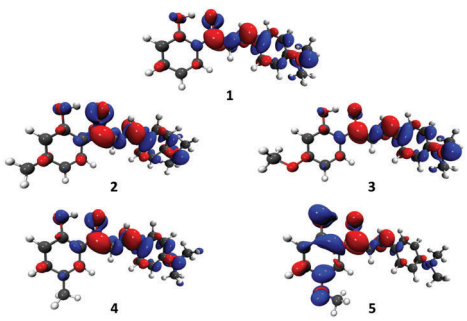

Fig. 3 Electron density difference maps (S_1–S_0) for **1–5**, showing where electron density has been transferred from in the ground state (blue) and transferred to in the excited state (red), calculated at ADC(2)/def2-TZVP level of theory.

For compound **5**, electron density is transferred not from the amine residue (**B**) but from the **A** fragment, due to the electron rich conjugation of the methoxy group (Fig. 3). Considerable electron density is transferred from O_P, increasing basicity and facilitating proton transfer. This results in a redshift of S_1 (0.1–0.2 eV, depending on the level of theory). Substitution does not affect the oscillator strengths significantly. Consequently, the first absorption band is very similar for all the compounds

(see Fig. S1 in the ESI†). In the case of **5**, the intensity of S_2 increases at expense of the S_1 oscillator strength with a small effect on the spectrum.

Excited state minima (E* and K*)

The minima in the first excited state (E* and K*) for all compounds were optimised using ADC(2) and CC2 methods. The energy of the E* state is sensitive to the position and electronic properties of the substituent. An EDG in *meta* (**2** and **3**) has a negligible effect on the energy of E*. If the substituent is in *para* (compounds **4** and **5**), no E* minimum can be located. For **1–3**, relaxation to a local minimum in E* is *via* intramolecular rotation. To describe this mode, we define the torsional rotation angle θ_{tor} (see Fig. 1).

Two E* minima can be found depending on the direction of rotation and in the case of **1**, both minima are equivalent. For the rest of compounds, the energy difference between these minima conformations is very small (<0.01 eV) and the two minima can be considered degenerate. Torsion through 180° results in *cis–trans* isomerisation, with the *trans* isomer about 1 eV less stable than *cis* in S_1. Consequently, *cis–trans* isomerisation is unlikely (ESI†).

For **1**, the E* minimum, θ_{tor} = 44° and a stabilisation of approximately 0.54 eV with respect to the FC geometry in S_1 (Fig. 2). Compounds **2** and **3** pass through a minimum, with θ_{tor} = 46° and 54° respectively. Potential energy curves and our non-adiabatic dynamic simulations show that ESIPT from this geometry is improbable. The emission energies from the E* state for **1**, **2** and **3** are 1.63, 1.59 and 1.46 eV respectively, which correspond to the IR region, where these compounds have shown fluorescence.[3]

In the K* state, where the proton has migrated, the system relaxes *via* intramolecular rotation about θ_{tor}. Two minima with very similar energies can be also located depending on the direction of rotation. The θ_{tor} value ranges between 40° and 60°. These minima are about 1 eV below the excitation energy corresponding to the FC geometry, and are more stable than E* minima. As such a bias towards the ESIPT mechanism can be expected.

An EDG in *para* (**4** and **5**) stabilises the K* S_1 state with respect to **1**, but the relative stabilisation with respect the S_1 energy for the FC geometry is quite similar for all the derivatives (about 1 eV). The emission from K* is in the range of 0.7–1.0 eV for all molecules in K*. S_1 energies (for K* and E*) with ADC(2) method are in good agreement the obtained with CC2 (within the 0.1–0.2 eV range). At the same time, the ADC(2) destabilises the K ground state with respect the CC2 method. This behaviour has consequences for the optimisation of MECI and the description of the S_0/S_1 crossing seam using the ADC(2) method, which are discussed in the next section.

Relaxation mechanisms and minimum energy conical intersections

Intramolecular rotation is a common relaxation pathway and has been reported previously in ESIPT chromophores, funnelling the system to the S_0/S_1 conical intersections.[15,23,27,50–53] For these molecules, the ground state is accessible *via* non-radiative channels from both E* and K* states (Fig. 4). We locate the corresponding S_0/S_1 MECI geometries for all compounds (**1–5**) at CC2/def2-TZVP, ADC(2)/def2-TZVP and ADC(2)/def2-SV(P) levels of theory (all energies and geometries can be found in the ESI†). Fig. 2 shows the relative energies of these structures at CC2/def2-TZVP level of theory.

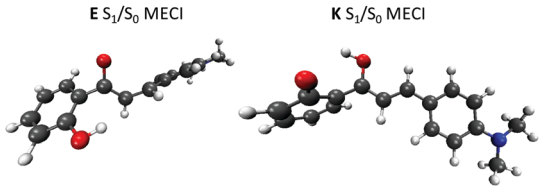

Fig. 4 MECI geometries for **1** optimised at CC2/def2-TZVP level of theory.

The molecules undergo intramolecular rotation in K* to reach a minimum. The same rotational mode is followed to reach the conical intersection seam and subsequent ground state reverse proton transfer to complete the photocycle. For **1**, the geometries were optimised with CC2 methods using the def2-SV(P) and def2-TZVP basis sets. For comparison, the conical intersections were also located with CASSCF(12,11)/6-31G(d) and CASSCF(14,13)/6-31G(d) levels of theory.

The geometry of the K S_1/S_0 MECI obtained with the CC2 method is in very good agreement with the obtained with CASSCF, θ_{tor} = 88° (89° with CASSCF method). Tuna *et al.* have shown that the CC2 method is able to describe the topology of the crossing seam between S_0 and S_1.[54] The RMSD deviation between both geometries is only 0.08 Å (ESI†). The geometries obtained with both basis sets are very similar.

For **1**, the MECI lies at only 0.02 eV above the K* minimum (Fig. 2). Substituents slightly increase the energy of the MECI (0.1–0.2 eV), but the MECIs are accessible during the relaxation. Linear interpolation pathways provide a maximum value for reaction barriers in the excited state (ESI†).[55] In the case of **1**, we optimise the intermediate states of the linear interpolated pathways at CC2/def2-TZVP level of theory, fixing the θ_{tor} angle (Fig. 5). The θ_{tor} = 50° for the K* minimum, a further

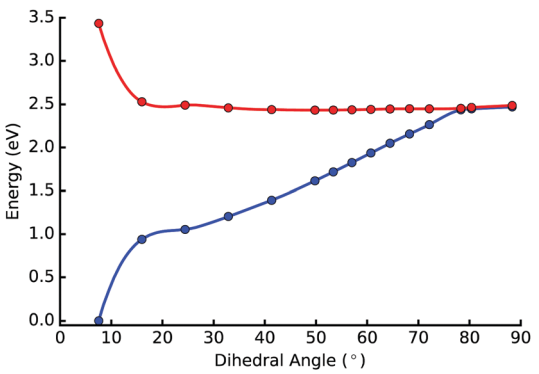

Fig. 5 Relaxed linear interpolation pathway obtained at CC2/def2-TZVP level of theory.

30° rotation takes the molecule to the MECI. In this region of the potential energy surface, the S_1 energy does not change significantly with θ_{tor}, which can be associated with an extended crossing seam as previously described by Robb *et al.* in an analogous ESIPT system.[56]

The frustration of intramolecular rotation in the solid state has been hypothesised to prevent access to a conical intersection, resulting in aggregation induced emission.[57,58] We observe similar results when the dihedral angle is fixed during K* optimization. The linear interpolation potential energy curves show that there is a stable K* region for **1** prior to the conical intersection, where emission could take place in the NIR region if the rotation is strongly hindered. The driving force behind the rotation is potentially the stabilisation of the dipole moment, which increases from 7.73 (S_0) to 13.32 D (E*) upon excitation. This is reduced to 3.99 D in the twisted conformation.

We did not observe significant barriers associated with the proton transfer for any of considered compounds (ESI†). The static calculations suggest that the relaxation process involves a proton transfer step followed by rotation around the θ_{tor} angle. The ESPIT is facilitated by the K* minimum, which is more stable for **4** and **5** (EDG in *para*). For compound **5**, the reaction coordinate is completely downhill and the K*/MECI geometry, correlating with intramolecular rotation. Experimentally, **4** and **5** do not show fluorescence either in solution or solid state. In the case of the solid state, the lack of fluorescence has been associated with the crystal packing.[3] Our calculations suggest that the character of the substituent might also play a role.

The ADC(2) geometries for the K S_0/S_1 MECI of all studied compounds show a θ_{tor} angle significantly deviated from CC2 and CASSCF values. The ADC(2) MECI structures are very similar to the K* minima (deviated about 10°). ADC(2) method does not properly describe the topology of the S_1/S_0 conical intersections.[54] This behaviour is associated with the description of S_0 with the MP2 method, which artificially destabilises S_0 and thus the S_0/S_1 crossing occurs at smaller angles. Similar results were found with def2-SV(P) and def2-TZVP basis sets.

For these systems, the S_1 potential energy surfaces obtained with ADC(2) are in a very good agreement with the CC2. Therefore, the ADC(2) method can be used to study the first steps of the excited state dynamics, but the results when the energy of S_0 and S_1 approaches must be analysed with care.

The non-ESIPT relaxation channel is also via intramolecular rotation in the E* state, leading to a second MECI. The stabilisation of these MECI structures involves relaxation through the θ_{tor} angle, which is significantly larger for **1** with a value of about 124° (θ_{tor} = 144° with CASSCF). For **1**, we also observed relaxation through the H–C–C–H dihedral angle (88°) (Fig. 4). For the rest of the S_1–S_0 MECI structures (**2–5**), only the θ_{tor} deviates from the plane. These differences are due to stabilisation of the dipole moment because of the EDG substituents.

For **1–3**, the E S_1–S_0 MECIs are slightly higher in energy than the E* minima (0.2–0.3 eV). Considering the small energy gap and the absence of barriers, the crossing seam region should be accessible. Another mechanism is the direct relaxation to the MECI from the FC geometry, which is the only possibility for **4** and **5**, considering the lack of a stable E* minimum. These calculations show that the competition between the ESPIT and the relaxation to E* will depend on the substituent. While in the case of **4–5**, a bias towards the ESPIT is expected, a more even distribution between both channels is likely. Non-adiabatic dynamic simulations confirm this analysis.

Non-adiabatic dynamic simulations

Compounds **1** and **5** represent the extreme cases, with most significant difference in the electronic structure of the excited states. The potential energy surfaces show that rotation about the θ_{tor} angle is activated during the stabilisation of the excited state minima (E* and K*). Surface hopping simulations allow analysis of the competition between different relaxation pathways and the role of rotation in the mechanism. The first steps of the photo-relaxation of **1** and **5** were explored using non-adiabatic dynamics considering two excited states (S_2 and S_1), which are close in energy (Table 1).

Our simulations confirm that the main deactivation pathways are associated with relaxation to the K* and E* minima. Both mechanisms involve the rotation about the θ_{tor} angle. In the case of **5**, the E* minimum close to the Franck–Condon geometry is not stable and the molecule relaxes directly to the MECI (Fig. 4). Relaxation to the K* minimum involves ESIPT. The competition between both reaction channels strongly depends on the substituent. In the case of **1**, both pathways are similarly populated (K*: 48%, E*: 52%). The population of the different pathways depends on the initial state; for trajectories started in S_2, the fraction is larger (K*: 60%, E*: 40%, ESI†). For **1**, the significant population of the E* channel is associated with the stabilisation of the E* minimum.

In our analysis, the proton transfer time was chosen to be the point at which the proton is equidistant between O_K and O_P. For **1** and **5**, the average time for the first proton transfer is 59 fs and 10 fs respectively. The analysis of the average distances and angles for all trajectories can be found in the ESI.† All trajectories exhibiting ESIPT (for **1** and **5**) found the ground state before the maximum simulation time (500 fs). We can identify three steps in the ESIPT mechanism. (I) Relaxation in the excited state (E* form). (II) Proton transfer (ESIPT). (III) Relaxation in K* followed by internal conversion. These three steps are illustrated for a typical trajectory in Fig. 6. During step I, the angle decreases to facilitate the proton transfer in II. In some trajectories, the proton is transferred back and forth (ESI†). In step III, the molecule relaxes in the keto form, resulting in most cases in the internal conversion to the ground state.

In this case, in step I, the molecule adopts a planar conformation (θ_{tor} = 11) to facilitate the proton transfer in step II. ESIPT occurs at 45 fs, after which dihedral rotation of −37° results in the conical intersection being reached after 139 fs. For **5**, the ESIPT occurs in 80% of the trajectories, showing a very similar channel preference regardless of the initial state.

Step III involves the relaxation of the angle, which reduces the S_0–S_1 gap leading to internal conversion. The region with S_0–S_1 gap of 0.1 eV is accessed in an average time of 76 fs post-ESPIT for **1** and 47 fs for **5**. Considering the features of the PES at ADC(2)/def2-SV(P) level of theory, these times are underestimated with

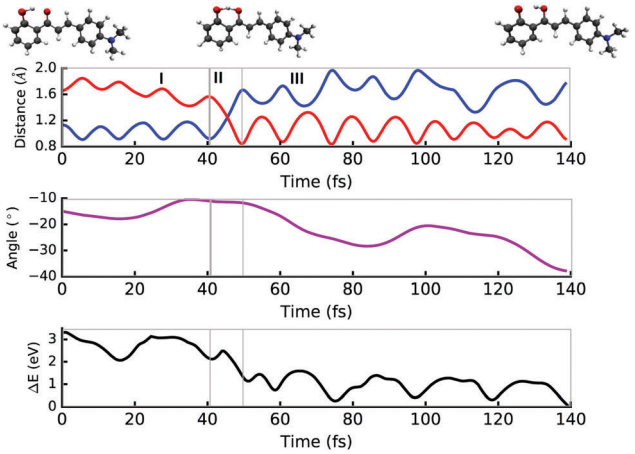

Fig. 6 The proton distance, dihedral angle and S_1–S_0 energy difference for a compound **1** trajectory exhibiting ESIPT. The time of ESIPT is denoted as when O_K–H bond length (red) = O_P–H (blue). The conical intersection is accessed after 139 fs, as θ_{tor} increases post proton transfer.

respect to real internal conversion times, but they provide an indication of how fast the molecules reach the crossing seam region, which is particularly extended for these molecules as shown in Fig. 5.

The mechanism *via* intramolecular rotation in E* compromises two steps: (I) Relaxation in the E* minimum, which is close to the Franck–Condon geometry. (II) Further relaxation leading to the internal conversion. Both processes involve the rotation around the angle θ_{tor}. Only 20% of the trajectories deactivated through this channel did not reach the S_1–S_0 < 0.1 eV region within the simulation time. In the case of **5**, where there is not a E* minimum close to the Franck–Condon geometry, the molecule relaxes directly to the crossing seam region. On average, the S_1–S_0 < 0.1 eV region is reached within an average time of 228 fs for **1** and 241 fs for **5**.

Fig. 7 shows a typical trajectory relaxing *via* intramolecular rotation in E*. The angle $\theta_{tor} = -10.5^\circ$ at 0 fs and for the first 110 fs of the simulation (step I), the angle oscillates about the equilibrium value (-11.0° at ADC(2)/def2-SV(P) level of theory).

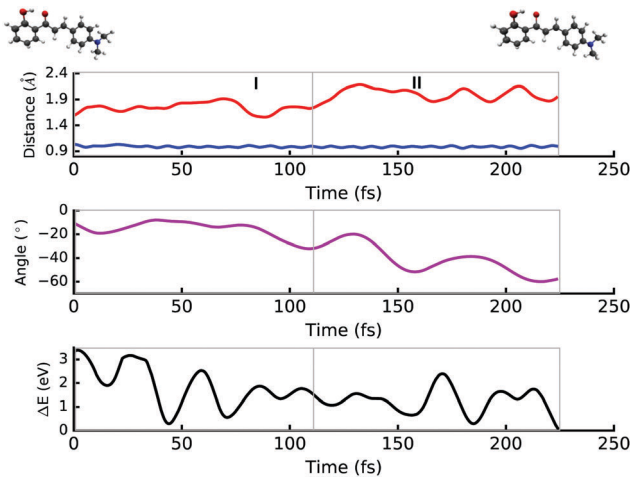

Fig. 7 Typical trajectory showing the relaxation in E*. The proton distance, dihedral angle and S_1–S_0 energy difference for compound **1**. Torsional rotation about θ_{tor} in E* prevents ESIPT.

Then, the rotation removes the C–O group from the plane prohibiting ESIPT and the molecule reaches the CI region at 225 fs, with $\theta_{tor} = -57.6^\circ$. The dynamics support the assertions from the potential energy curves that proton transfer from the twisted E* form, with a barrier of 1.2 eV (see ESI†), is improbable. Relaxation in E* therefore competes with ESIPT in compound **1** due to the close proximity of a local minimum close to the Franck–Condon geometry. Proton transfer followed by internal conversion is the faster process, with an average time duration of 123 fs, compared to 228 fs for rotation in E*.

Our dynamic simulations do not allow the prediction of post-internal conversion behaviour, but the analysis of the PES can help understand the following steps in the mechanisms. Post-ESIPT, two relaxation pathways are possible once the MECI is populated. The first completes the four-level photocycle and returns the system to the ground state *cis*-enol form *via* ground state reverse proton transfer (Fig. 2). The second continues the rotation about θ_{tor} to produce the *trans*-keto form of 2′-hydroxychalcone.[9]

Following internal conversion, the system in the ground state can populate the *cis* or *trans* forms (-enol or *trans*-keto forms). Rotation will favour the *cis* form, which is stabilised by the $O_P\cdots H\cdots O_K$ hydrogen bond. The *trans*-keto ground state lies 1.15 eV (MP2/def2-TZVP) above the *cis*-enol ground state, consequently we expect a larger population of the *cis* products (ESI†).

Our non-adiabatic dynamics simulations clearly illustrate the effect of a strong electron donor in the *para* position on the ESIPT process in 2′-hydroxychalcones. The population of the ESIPT channel and rate of proton transfer is greatly increased.

Conclusions

We have applied state-of-the-art computational methods to investigate the photochemistry of five derivatives of 2′-hydroxychalcone, an ESIPT-active compound with potential application in organic lasers and optoelectronics. Experimental data show that 2′-hydroxychalcones are non-emitting in solution and only fluoresce through AIE.[28] Our calculations provide theoretical description of the ESIPT process and subsequent relaxation mechanisms of 2′-hydroxychalcones in gas phase, which represents the first step for the understanding of the photochemistry of these systems.

Through calculation of vertical excitation energies and corresponding absorption spectra, we find that electron donating groups have a minimal influence of the absorption characteristics of 2′-hydroxychalcone. It takes a strong electron donor in the *para* position to alter the vertical excitation energy, on account of the increased conjugated electron density. On the other hand, relaxation back to the ground state is far more sensitive to the electron donating power of the substituent and its positioning on the phenol moiety. The *para* position is more sensitive than *meta*, where the same effect is seen even with methyl. Dual-emission is thus inhibited with a strong EDG in 2′-hydroxychalcones. This is quite unexpected, with a comprehensive study on the effects of substituents in common ESIPT-compounds finding that electron donating groups in any position favour the E* form.[59]

We found that the ground state is accessible *via* non-radiative channels from both E* and K* states. S_0/S_1 MECI structures were found for all compounds, associated with an extended crossing seam. Both mechanisms involve the activation of an intermolecular rotation mode (about the θ_{tor} angle). The competition between both mechanisms depends strongly on the position and nature of the substituent of the substituent. Proton transfer is more favourable with electron donating groups in *para*, correlating with donating power. Non-adiabatic surface-hopping dynamic simulations provide a full picture of relaxation energetics and timescales.

ESPIT is strongly favoured for **4–5**, where there are not stable E* minima. For compound **5**, the reaction coordinate is completely downhill correlating with intramolecular rotation. Our dynamic simulations show a bias towards the K* relaxation mechanism. Experimentally, **4** and **5** does not fluoresce either in solution or solid state. Wang *et al.* suggested that for the solid material, this behaviour is related to the crystal packaging.[3] Our calculations show that the character of the substituent and the electronic effects in the monomers might also play a role in the mechanism. Further calculations have been carried out in solid state to confirm this hypothesis. Our results contribute to a better understanding of photochemistry of isolated AIE chromophores that could help design more efficient solid state emitters.

Acknowledgements

The calculations were performed using the Queen Mary's MidPlus computational facilities supported by QMUL Research-IT and funded by EPSRC grant EP/K000128/1 and the Slater HPC facility from the National Service for Computational Chemistry Software (NSCCS). The authors acknowledge the support from the School of Biological and Chemical Sciences at Queen Mary University of London.

References

1 D. Oushiki, H. Kojima, T. Terai, M. Arita, K. Hanaoka, Y. Urano and T. Nagano, *J. Am. Chem. Soc.*, 2010, **132**, 2795–2801.
2 N. Karton-Lifshin, E. Segal, L. Omer, M. Portnoy, R. Satchi-Fainaro and D. Shabat, *J. Am. Chem. Soc.*, 2011, **133**, 10960–10965.
3 S. Wang, X. Yan, Z. Cheng, H. Zhang, Y. Liu and Y. Wang, *Angew. Chem., Int. Ed.*, 2015, **54**, 13068–13072.
4 A. S. Klymchenko and A. P. Demchenko, *Phys. Chem. Chem. Phys.*, 2003, **5**, 461–468.
5 D. A. Yushchenko, V. V. Shvadchak, A. S. Klymchenko, G. Duportail, V. G. Pivovarenko and Y. Mély, *J. Phys. Chem. A*, 2007, **111**, 10435–10438.
6 N. Kungwan, F. Plasser, A. J. A. Aquino, M. Barbatti, P. Wolschann and H. Lischka, *Phys. Chem. Chem. Phys.*, 2012, **14**, 9016–9025.
7 R. Daengngern and N. Kungwan, *Chem. Phys. Lett.*, 2014, **609**, 147–154.
8 A. P. Demchenko, K.-C. Tang and P.-T. Chou, *Chem. Soc. Rev.*, 2013, **42**, 1379–1408.
9 V. S. Padalkar and S. Seki, *Chem. Soc. Rev.*, 2015, **45**, 169–202.
10 J. E. Kwon and S. Y. Park, *Adv. Mater.*, 2011, **23**, 3615–3642.
11 J. Zhao, S. Ji, Y. Chen, H. Guo and P. Yang, *Phys. Chem. Chem. Phys.*, 2012, **14**, 8803.
12 X.-F. Yang, Q. Huang, Y. Zhong, Z. Li, H. Li, M. Lowry, J. O. Escobedo and R. M. Strongin, *Chem. Sci.*, 2014, **5**, 2177.
13 M. R. Rao, C.-W. Liao, W.-L. Su and S.-S. Sun, *J. Mater. Chem. C*, 2013, **1**, 5491.
14 D.-E. Wu, Q.-C. Yao and M. Xia, *Phys. Chem. Chem. Phys.*, 2015, **17**, 3287–3294.
15 M. Cai, Z. Gao, X. Zhou, X. Wang, S. Chen, Y. Zhao, Y. Qian, N. Shi, B. Mi, L. Xie and W. Huang, *Phys. Chem. Chem. Phys.*, 2012, **14**, 5289.
16 X. Du, J. Qi, Z. Zhang and Z. Y. Wang, *Chem. Mater.*, 2012, **24**, 2178–2185.
17 J. Mei, Y. Hong, J. W. Y. Lam, A. Qin, Y. Tang and B. Z. Tang, *Adv. Mater.*, 2014, **26**, 5429–5479.
18 C. C. Hsieh, P. T. Chou, C. W. Shih, W. T. Chuang, M. W. Chung, J. Lee and T. Joo, *J. Am. Chem. Soc.*, 2011, **133**, 2932–2943.
19 Y. Hong, J. W. Y. Lam and B. Z. Tang, *Chem. Commun.*, 2009, 4332.
20 A. Prlj, N. Došlić and C. Corminboeuf, *Phys. Chem. Chem. Phys.*, 2016, **18**, 11606–11609.
21 P. Chou, M. L. Martinez and W. C. Cooper, *J. Am. Chem. Soc.*, 1992, **114**, 4943–4944.
22 T. Teshima, M. Takeishi and T. Arai, *New J. Chem.*, 2009, **33**, 1393.
23 Y. Norikane, H. Itoh and T. Arai, *J. Phys. Chem. A*, 2002, **106**, 2766–2776.
24 T. Arai and Y. Norikane, *Chem. Lett.*, 1997, 339.
25 Z. Song, R. T. K. Kwok, E. Zhao, Z. He, Y. Hong, J. W. Y. Lam, B. Liu and B. Z. Tang, *ACS Appl. Mater. Interfaces*, 2014, **6**, 17245–17254.
26 X. Jin, L. Dong, X. Di, H. Huang, J. Liu, X. Sun, X. Zhang and H. Zhu, *RSC Adv.*, 2015, **5**, 87306–87310.
27 Y. Norikane, N. Nakayama, N. Tamaoki, T. Arai and U. Nagashima, *J. Phys. Chem. A*, 2003, **107**, 8659–8664.
28 X. Cheng, K. Wang, S. Huang, H. Zhang, H. Zhang and Y. Wang, *Angew. Chem., Int. Ed.*, 2015, **54**, 8369–8373.
29 F. Haase and R. Ahlrichs, *J. Comput. Chem.*, 1993, **14**, 907–912.
30 F. Weigend and R. Ahlrichs, *Phys. Chem. Chem. Phys.*, 2005, **7**, 3297.
31 A. Schäfer, H. Horn and R. Ahlrichs, *J. Chem. Phys.*, 1992, **97**, 2571.
32 O. Christiansen, H. Koch and P. Jorgensen, *Chem. Phys. Lett.*, 1995, **243**, 409–418.
33 C. Hättig and A. Köhn, *J. Chem. Phys.*, 2002, **117**, 6939–6951.
34 C. Hättig and F. Weigend, *J. Chem. Phys.*, 2000, **113**, 5154–5161.
35 A. Köhn and C. Hättig, *J. Chem. Phys.*, 2003, **119**, 5021–5036.
36 C. Hättig, *Adv. Quantum Chem.*, 2005, **50**, 37–60.
37 R. Ahlrichs, M. Bär, M. Häser, H. Horn and C. Kölmel, *Chem. Phys. Lett.*, 1989, **162**, 165–169.
38 B. G. Levine, J. D. Coe and T. J. Martínez, *J. Phys. Chem. B*, 2008, **112**, 405–413.
39 R. Crespo-Otero, N. Kungwan and M. Barbatti, *Chem. Sci.*, 2015, **6**, 5762–5767.

40 H. Werner, P. J. Knowles, G. Knizia, F. R. Manby and M. Schütz, *Wiley Interdiscip. Rev.: Comput. Mol. Sci.*, 2012, **2**, 242–253.
41 R. Crespo-Otero and M. Barbatti, *Theor. Chem. Acc.*, 2012, **131**, 1237.
42 M. Barbatti, M. Ruckenbauer, F. Plasser, J. Pittner, G. Granucci, M. Persico and H. Lischka, *Wiley Interdiscip. Rev.: Comput. Mol. Sci.*, 2014, **4**, 26–33.
43 M. Barbatti, G. Granucci, M. Ruckenbauer, F. Plasser, R. Crespo-Otero, J. Pittner, M. Persico and H. Lischka, *NEWTON-X: a package for Newtonian dynamics close to the crossing seam*, version 2.0, 2016, http://www.newtonx.org.
44 M. Barbatti, G. Granucci, M. Persico, M. Ruckenbauer, M. Vazdar, M. Eckert-Maksić and H. Lischka, *J. Photochem. Photobiol., A*, 2007, **190**, 228–240.
45 M. Barbatti, A. J. A. Aquino and H. Lischka, *Phys. Chem. Chem. Phys.*, 2010, **12**, 4959.
46 F. Plasser, R. Crespo-Otero, M. Pederzoli, J. Pittner, H. Lischka and M. Barbatti, *J. Chem. Theory Comput.*, 2014, **10**, 1395–1405.
47 I. G. Ryabinkin, J. Nagesh and A. F. Izmaylov, *J. Phys. Chem. Lett.*, 2015, **6**, 4200–4203.
48 L. Stojanović, S. Bai, J. Nagesh, A. Izmaylov, R. Crespo-Otero, H. Lischka and M. Barbatti, *Molecules*, 2016, **21**, 1603.
49 M. Barbatti and R. Crespo-Otero, *Top. Curr. Chem.*, 2015, **368**, 415–444.
50 Z. R. Grabowski, K. Rotkiewicz and W. Rettig, *Chem. Rev.*, 2003, **103**, 3899–4031.
51 M. Barbatti, A. J. a Aquino, H. Lischka, C. Schriever, S. Lochbrunner and E. Riedle, *Phys. Chem. Chem. Phys.*, 2009, **11**, 1406–1415.
52 S. Kim, J. Seo and S. Y. Park, *J. Photochem. Photobiol., A*, 2007, **191**, 19–24.
53 V. C. Víctor, *J. Phys. Chem. A*, 2004, **108**, 281–288.
54 D. Tuna, D. Lefrancois, L. Wolanski, S. Gozem, I. Schapiro, T. Andruniow, A. Dreuw and M. Olivucci, *J. Chem. Theory Comput.*, 2015, **11**, 5758–5781.
55 R. Crespo-Otero, A. Mardyukov, E. Sanchez-Garcia, M. Barbatti and W. Sander, *ChemPhysChem*, 2013, **14**, 827–836.
56 M. J. Paterson, M. A. Robb, A. Lluís Blancafort and A. D. DeBellis, *J. Phys. Chem. A*, 2005, **109**, 7527–7537.
57 X.-L. Peng, S. Ruiz-Barragan, Z.-S. Li, Q.-S. Li and L. Blancafort, *J. Mater. Chem. C*, 2016, **4**, 2802–2810.
58 Q. Li and L. Blancafort, *Chem. Commun.*, 2013, **49**, 5966–5968.
59 C. Azarias, Š. Budzák, A. D. Laurent, G. Ulrich and D. Jacquemin, *Chem. Sci.*, 2016, **7**, 3763–3774.

